

Supplementary Information

Conductance of metal superatom-based molecular wires influenced by nanoscale effects

Famin Yu,^{abc} Wei Feng^c, Baiqiang Liu^b, Rui-Qin Zhang^{*d} and Zhigang Wang^{*bc}

^a School of Physics, Changchun Normal University, Changchun 130032, China.

^b Key Laboratory of Material Simulation Methods & Software of Ministry of Education, College of Physics, Jilin University, Changchun 130012, China. *E-mail: wangzg@jlu.edu.cn (Z. W.)

^c Institute of Atomic and Molecular Physics, Jilin University, Changchun 130012, China.

^d Department of Physics, City University of Hong Kong, Kowloon 999077 Hong Kong SAR, China.

*E-mail: aprqz@cityu.edu.hk (R. Z.)

1. Computational details

The W@Cu₁₂ quasi-1D SMWs were optimized using density functional theory (DFT) in Dmol³ software. The Perdew-Burke-Ernzerhof (PBE) functional within Generalized Gradient Approximation (GGA)¹ was used to treat the exchange-correlation functional² and the Double Numerical plus polarization (DNP) basis set was applied. Electrons within superatoms follow the same quantum mechanical principles as those within standard atoms, such as the Pauli Exclusion Principle and Hund's Rule,^{3, 4} which influence the distribution of electrons across various energy levels. The orbital shapes and symmetries of electrons in superatoms can be described using quantum mechanical wave functions. Furthermore, in superatomic assemblies, electrons occupy discrete energy levels akin to the electronic states in individual atoms.^{5, 6} These energy levels are dictated by quantum confinement and electron-electron interactions within the system. Therefore, the W@Cu₁₂ superatomic assembly which exhibits quantum properties is appropriately described using quantum mechanical methods for electrical conductivity analysis. To study tunneling conductance in small-scale electronic devices, the Non-Equilibrium Green's Function method coupled with Density Functional Theory (NEGF-DFT) within the DFT implemented by the Nanodcal software⁷ is chosen. This approach is a well-established ab initio technique extensively utilized for computing tunneling conductance,⁸⁻¹¹ with many studies validating its effectiveness in capturing experimental phenomena.^{7, 12, 13} Thus, this research is built upon a validated computational framework suitable for superatomic assemblies, ensuring the reliability of the tunneling conductance calculations.

Considering the assemblies examined in this study involve a substantial number of atoms, with the largest configuration comprising 416 atoms, to achieve a good balance between the computational feasibility and the accuracy of results, the semi-local functional was chosen. While range-separated functionals can provide more precise predictions of the highest occupied molecular orbital (HOMO) – the lowest unoccupied molecular orbital (LUMO) gap,^{14, 15} the most reliable approach for determining range-separation parameters involves comparison of computational results with experimental data.^{16, 17} In the case of the W@Cu₁₂ assemblies investigated in this study, the CCSD(T) method is computationally challenging, and experimental synthesis has not yet been performed. Thus, setting range-separation parameters based on references from other systems may introduce additional

uncertainties specific to systems studied in this research. In contrast, semi-local functionals are less dependent on specific parameters and exhibit broader applicability. Additionally, the $W@Cu_{12}$ molecular wires, composed of transition metals with the W atom having nearly half-filled d orbitals, exhibit significant static correlation.^{18, 19} Research shows that for such systems, pure functionals often yield more accurate results than hybrid functionals with Hartree-Fock components, which can over-correct HOMO-LUMO gaps.²⁰⁻²² Therefore, selecting a semi-local functional is more appropriate than RSH functionals, which struggle to tune the ω parameter for these systems.

Additionally, previous studies on $W@Au_{12}$ (a congener of $W@Cu_{12}$ in coinage metal superatom family) reveal that PBE-calculated HOMO-LUMO gaps (1.75-1.79 eV) show excellent consistency with experimental values (1.68 eV),^{5, 6, 23} with minimal deviation of 4-6%. Crucially, the homologous $d^{10}s^1$ electronic configurations of Cu and Au, coupled with identical superatomic orbital filling patterns in both $W@Cu_{12}$ and $W@Au_{12}$, establish fundamental electronic structure homology. This structural equivalence provides a solid theoretical basis for extending the validated PBE methodology from $W@Au_{12}$ to $W@Cu_{12}$, particularly given the absence of direct experimental data for the latter system. Nevertheless, the single-point calculations using both semi-local and RSH functionals on $W@Cu_{12}$ monomer and dimer were performed to compare HOMO-LUMO gaps and DOS, utilizing Gaussian 09 software package.²⁴ For $W@Cu_{12}$, PBE-derived HOMO-LUMO gap calculations yield 1.50 eV, aligning remarkably with both experimental measurements and PBE-based theoretical predictions established for its $W@Au_{12}$ counterpart in the coinage metal superatom family. This contrasts sharply with LC- ω PBE's prediction of 6.54 eV, which significantly exceeds experimentally accessible ranges for such systems and reveals inadequate static correlation effect treatment. This finding confirms the superior suitability of the PBE functional for accurately describing the electronic structure of $W@Cu_{12}$ systems. Despite differences in calculated HOMO-LUMO gaps, the DOS trends remain consistent, indicating that the overall electronic structure of $W@Cu_{12}$ wires is independent of functional choice. These supports using semi-local functionals to describe conductance trends with length, as shown in Figure S2. Furthermore, semi-local and even local functionals can capture similar electronic transport trends as RSH functionals.^{14, 25} Several studies have successfully used semi-local functionals to describe experimental phenomena,^{13, 26} providing strong support for this choice in our work.

Therefore, the semi-local functional was chosen in this work. Therefore, in the NEGF-DFT calculation, GGA-PBE96 was used for the exchange-correlation functional, and the double- ζ plus polarization (DZP) basis set was used for all atoms. We used a two-probe model which comprises three parts: left and right electrodes (which extend to $\pm \infty$) plus central scattering region. Furthermore, given that increasing the assembly units laterally can effectively narrow the energy gap between HOMO and LUMO^{27, 28}, potentially enhancing electrical transport properties, we also conducted research into the transport characteristics of SMWs formed by laterally expanded $W@Cu_{12}$ monomers. The distance between the central scattering region and the electrodes was maintained at 2.5 Å for different quasi-1D $W@Cu_{12}$ SMWs to minimize differences in the electrode-scattering region coupling, which contributes to a clearer understanding of the physics arising from the device length. Vacuum layers in the y and z directions exceeding 10 Å were adopted to eliminate interactions between neighboring cells. The cutoff energy was set to 80 Hartree, the temperature of electrodes was chosen as 300 K and the k-point grid of electrodes was set to $1 \times 1 \times 100$.

2. Computational model of quasi-1D SMWs.

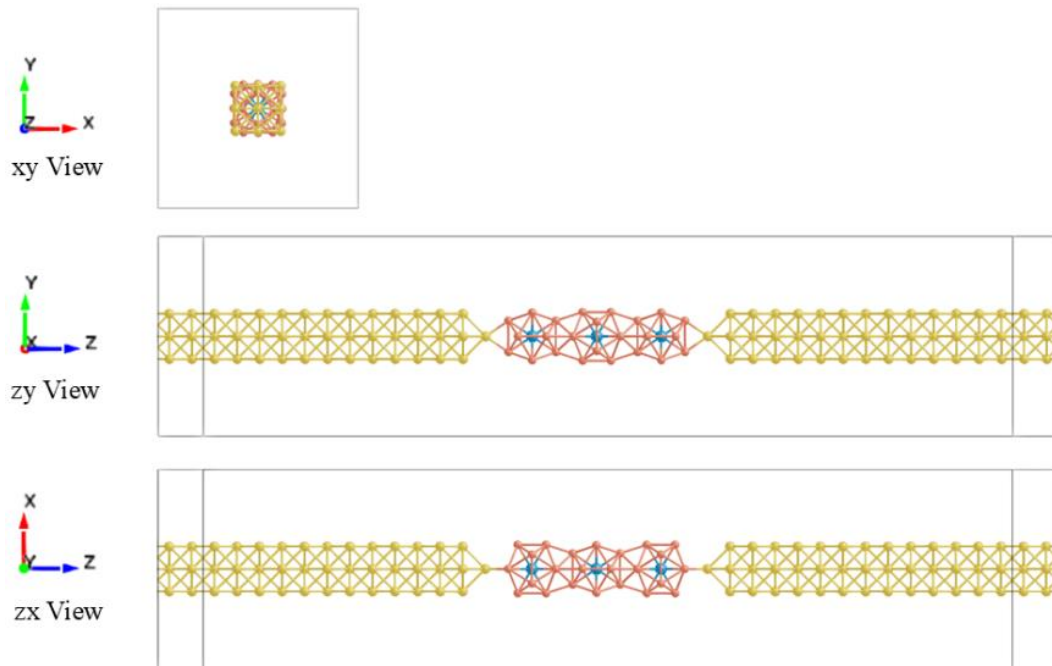


Figure S1. Computational model of quasi-1D SMWs, illustrated using a 1x3 system as an example.

3. Conductance of W@Cu₁₂ superatom assemblies.

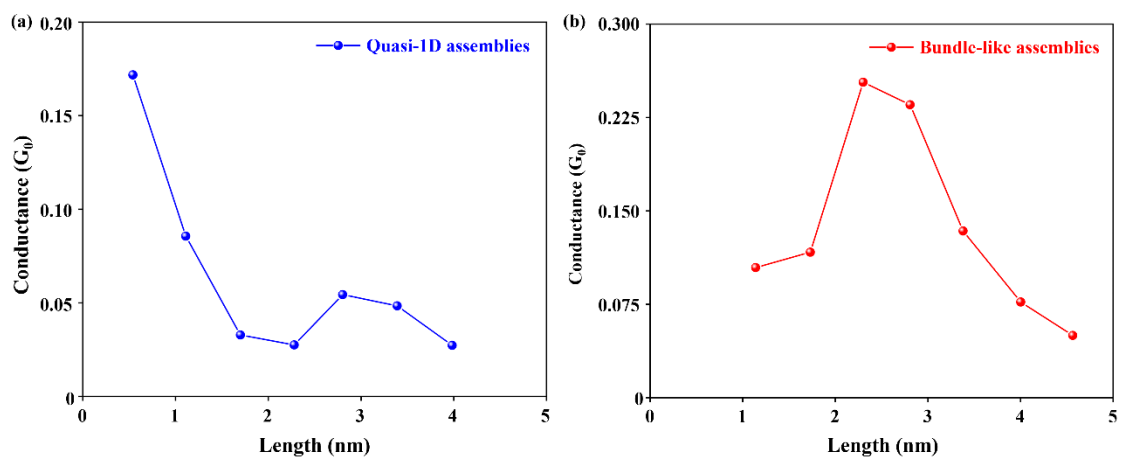


Figure S2. Conductance of W@Cu₁₂ superatom assemblies. (a) Conductance of quasi-1D assemblies with different length. (b) Conductance of bundle-like assemblies with different length.

4. Error analysis of the fitted parameter β .

The discrepancy between the fitted β values and experimental values stems from three primary factors. First, the limited data present inherent statistical challenges. The anomalous conductance phenomena observed in superatomic molecular wires below 2.5 nm were documented with only four data points in quasi-one-dimensional configurations and three data points in bundle-like configurations. This scarcity introduces sampling bias, thereby expanding the error margins in parameter estimation. Second, systematic uncertainties arise from the linear fitting procedure itself, which may inadequately capture the complex quantum effect dependencies. Consequently, the fitted β values exhibit deviations from experimental measurements.²⁹ Third, the neglect of surface reconstruction effects in semi-infinite periodic electrode models may introduce systematic deviations in interfacial electronic structure. The confluence of these factors introduces error margins. Furthermore, considering the relative stability of the boundary geometric structure during the extension of superatomic molecular wires, the aforementioned error sources primarily affect the absolute magnitude of β values rather than their relative trend with length variation.

5. Computational model of quasi-1D SMWs.

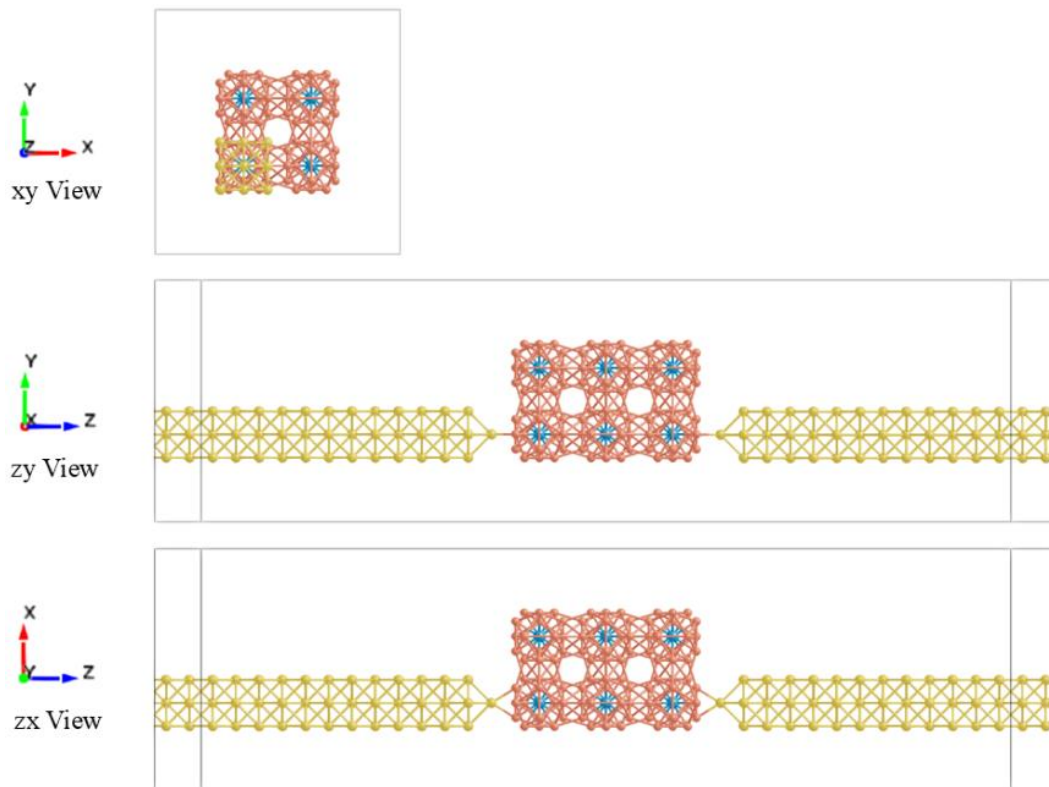


Figure S3. Computational model of bundle-like SMWs, illustrated using a $2 \times 2 \times 3$ system as an example.

6. Calculated density of states for W@Cu₁₂ monomer and dimer.

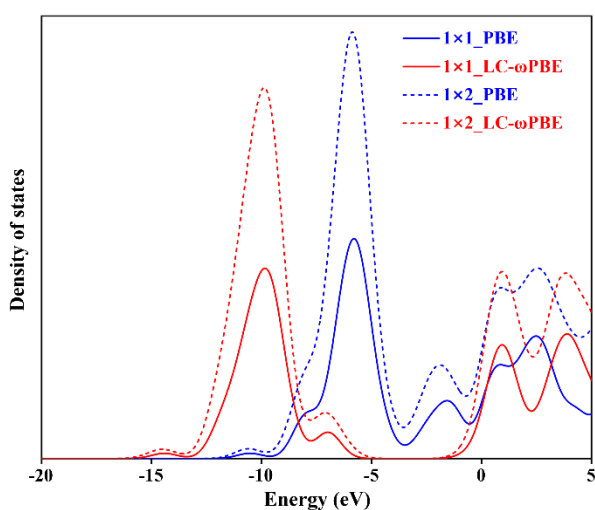


Figure S4. Calculated density of states for W@Cu₁₂ monomer and dimer using PBE and LC- ω PBE functionals, respectively.

In order to investigate the conductance trend under different functionals, the single-point calculations using the semi-local functionals PBE and LC- ω PBE on the W@Cu₁₂ monomer and dimer were performed. The HOMO – LUMO gaps calculated by PBE for the monomer and dimer are 1.50 eV and 0.73 eV, respectively, while LC- ω PBE yields 6.54 eV and 5.39 eV, respectively. This difference arises from the tendency of semi-local functionals to underestimate band gaps, while hybrid functionals tend to overestimate them in transition metal systems. Nonetheless, the primary focus of this research is the trend of conductance with length, emphasizing changes in the overall electronic structure. We further analyzed the DOS for the monomer and dimer under both functionals. As shown in Figure S4, comparing HOMO-LUMO gaps of the monomer or dimer reveals that the main difference between the two functionals lies in the size of the HOMO-LUMO gap, while the overall trend of the DOS curve remains consistent. Moreover, comparing the DOS of the monomer and dimer under the same functional shows a consistent trend in their curves. This consistency suggests that, although there are variations in conductance values due to differences in the HOMO-LUMO gaps calculated by different functionals, the broad features and overall trends in the electronic structure of the W@Cu₁₂ molecular wire appear to be relatively consistent across the functionals used.

7. Scattering states analyses.

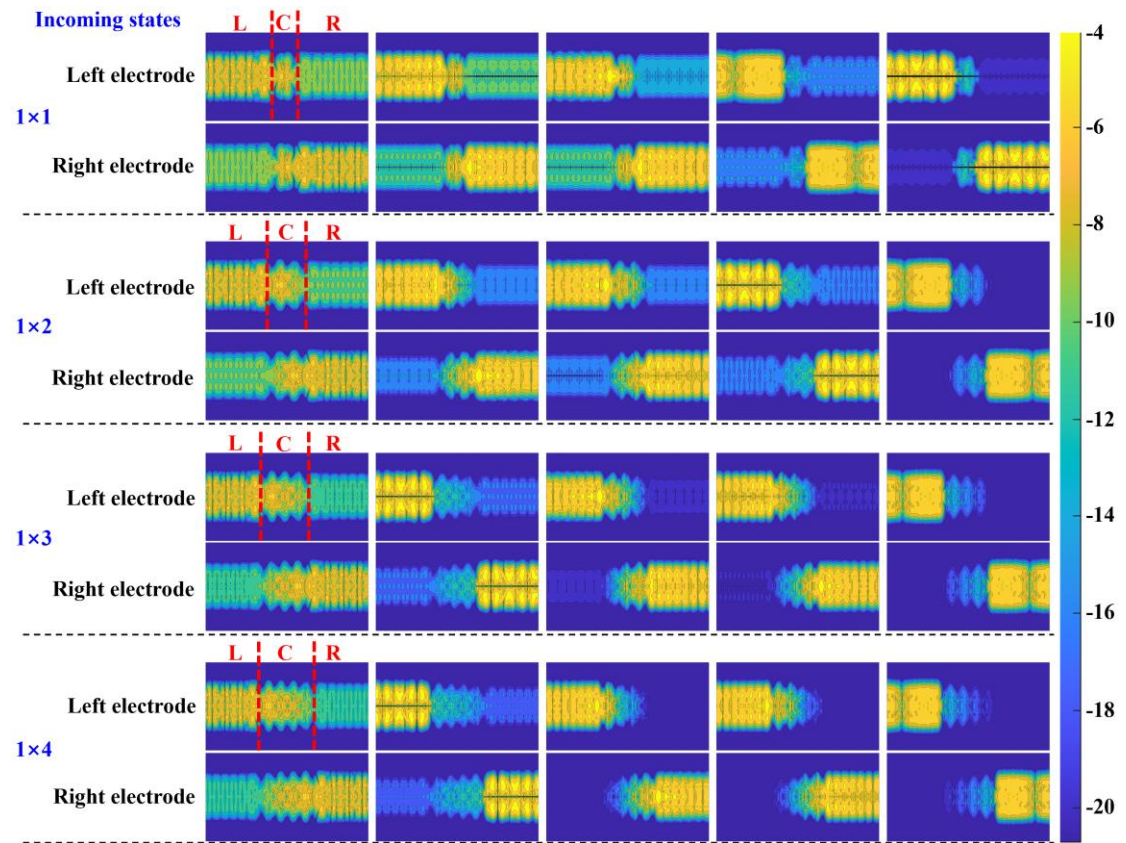


Figure S5. Real-space scattering states at E_F of quasi-1D SMWs. L, C, and R represent the left electrode, the central scattering region, and the right electrode, respectively.

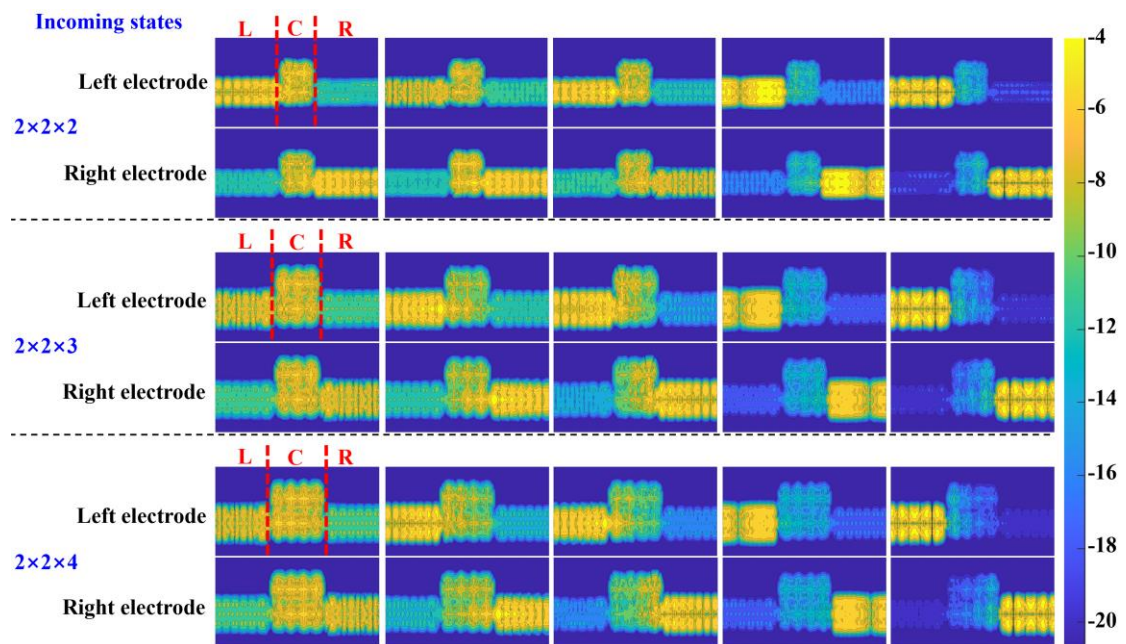


Figure S6. Real-space scattering states at E_F of bundle-like SMWs. L, C, and R represent the left electrode, the central scattering region, and the right electrode, respectively.

References

1. J. P. Perdew, K. Burke and M. Ernzerhof, *Phys. Rev. Lett.*, 1996, **77**, 3865-3868.
2. J. Paier, R. Hirschl, M. Marsman and G. Kresse, *J. Chem. Phys.*, 2005, **122**, 234102.
3. V. M. Medel, J. U. Reveles, S. N. Khanna, V. Chauhan, P. Sen and A. W. Castleman, *Proc. Natl. Acad. Sci. U. S. A.*, 2011, **108**, 10062-10066.
4. X. Wu, F. Yu, W. Xie, Z. Liu, Z. Wang and S. Zhang, *J. Phys. Chem. Lett.*, 2022, **13**, 2632-2637.
5. Q. Du, Z. Wang, S. Zhou, J. Zhao and V. Kumar, *Phys. Rev. Mater.*, 2021, **5**, 066001.
6. F. Yu, Y. Zhu, Y. Gao, R. Wang, W. Huang, Y. Gao and Z. Wang, *Nano Res.*, 2022, **15**, 8665-8672.
7. J. Taylor, H. Guo and J. Wang, *Phys. Rev. B*, 2001, **63**, 245407.
8. Q. An, C. Hu, G. H. Yu and H. Guo, *Nanoscale*, 2020, **12**, 6079-6088.
9. H. Liu, N. Wang, J. Zhao, Y. Guo, X. Yin, F. Y. C. Boey and H. Zhang, *ChemPhysChem*, 2008, **9**, 1416-1424.
10. Y. R. Chen, K. Y. Chen, K. P. Dou, J. S. Tai, H. H. Lee and C. C. Kaun, *Carbon*, 2015, **94**, 548-553.
11. Z.-X. Yin, Y.-D. Li, Y.-H. Ye, Y. Liu, M.-F. Li, Z.-J. Yang, X.-R. Zheng, H.-Z. Wang, Y. Wang and Y.-D. Deng, *Rare Met.*, 2024, **43**, 5781-5791.
12. Y. Zhao, Y. Hu, L. Liu, Y. Zhu and H. Guo, *Nano Lett.*, 2011, **11**, 2088-2091.
13. Y. Gao, K. Shen, P. Liu, L. Liu, F. Chi, X. Hou and W. Yang, *Front. Phys.*, 2021, **8**, 616066.
14. S. Bhandari, A. Yamada, A. Hoskins, J. Payne, H. Aksu and B. D. Dunietz, *Adv. Theory Simul.*, 2021, **4**, 2000016.
15. M. E. Foster and B. M. Wong, *J. Chem. Theory Comput.*, 2012, **8**, 2682-2687.
16. T. Körzdörfer, J. S. Sears, C. Sutton and J.-L. Brédas, *J. Chem. Phys.*, 2011, **135**, 204107.
17. É. Brémond, Á. J. Pérez-Jiménez, J. C. Sancho-García and C. Adamo, *J. Chem. Phys.*, 2020, **152**, 244124.
18. K. P. Kepp, *Coord. Chem. Rev.*, 2013, **257**, 196-209.
19. J. W. Hollett and P. M. W. Gill, *J. Chem. Phys.*, 2011, **134**, 114111.
20. J. N. Harvey, *Annual Reports Section "C" (Physical Chemistry)*, 2006, **102**, 203-226.
21. J. P. Wang, W. Y. Xie, W. R. Jiang, X. C. Wu and Z. G. Wang, *Adv. Theory Simul.*, 2019, **2**, 1900138.
22. X. Dai, Y. Gao, M. Xin, Z. Wang and R. Zhou, *J. Chem. Phys.*, 2014, **141**, 244306.
23. X. Li, B. Kiran, J. Li, H. J. Zhai and L. S. Wang, *Angew. Chem. Int. Ed.*, 2002, **41**, 4786-4789.
24. M. J. Frisch, G. W. Trucks, H. B. Schlegel and G. E. Scuseria, *Wallingford CT*, 2009.
25. D. P. Jelenfi, A. Tajti and P. G. Szalay, *J. Chem. Phys.*, 2025, **162**, 034101.
26. A. K. Paul, M. Kuri, D. Saha, B. Chakraborty, S. Mahapatra, A. K. Sood and A. Das, *npj 2D Materials and Applications*, 2017, **1**, 17.
27. J. T. Arantes and A. Fazzio, *Nanotechnology*, 2007, **18**, 295706.
28. H. J. Xiang, J. Yang, J. G. Hou and Q. Zhu, *Appl. Phys. Lett.*, 2006, **89**, 223111.
29. E. Leary, B. Limburg, A. Alanazy, S. Sangtarash, I. Grace, K. Swada, L. J. Esdaile, M. Noori, M. T. González, G. Rubio-Bollinger, H. Sadeghi, A. Hodgson, N. Agraït, S. J. Higgins, C. J. Lambert, H. L. Anderson and R. J. Nichols, *J. Am. Chem. Soc.*, 2018, **140**, 12877-12883.